On the Mode-Coupling Instability of Mechanical Systems Due to Sliding Friction Constraint

S. Chatterjee

Department of Mechanical Engineering, Bengal Engineering and Science University, Shibpur, P.O. Botanic Garden, Howrah-711 103, West Bengal, India

(Received 2 March 2006; revised 23 June 2006; accepted 13 October 2006)

A general lumped parameter model with two modes of vibration coupled through sliding friction constraint is considered. Stability analysis is carried out considering perfectly rigid and compliant contact models. The linear viscoelastic model and the non-linear Hunt-Crossley model of compliant contact are used to study the influence of the model of contact damping on stability. Influences of the contact parameters and the ratio of the modal parameters on the stability of sliding have been discussed in details. Mainly, three types of instabilities specifically, low-frequency flutter, high-frequency flutter, and divergence are found to exist in the class of systems considered. The condition of the existence of high-frequency flutter is shown to coincide with the condition of the Painleve paradox. Perfectly rigid contact consideration fails to provide qualitative as well as quantitative description of sliding instability in a specific parameter zone, where only a compliant contact model can properly describe the instability phenomenon. For low contact damping, stability boundary obtained from the perfectly rigid contact consideration is not the limit of that obtained from a compliant contact model, even with very high contact stiffness. Contact damping plays an important role in ascertaining the shape, size, and characteristics of the stability boundary.

1. INTRODUCTION

Friction induced instability in elastic systems has received serious attention from a large number of researchers. Several seminal review articles on the topic are available.[1-3] Depending upon the mechanisms involved, friction induced sliding instability may be broadly classified into two categories: 1) instability induced by the Stribeck effect and 2) mode-coupling instability. The central focus of the present article is on a particular type of mode-coupling instability, which goes by the name of 'kinematic constraint instability' in early literature. The term 'kinematic constraint instability' is relevant only for perfectly rigid contact assumption, where the contact boundaries are viewed as the rigid constraints to the motion. In reality, any contact surface involves elastic deformation, however small this may be. Thus, contact force emerges as the coupling force among the different modes of vibration of a sliding elastic structure. Several early studies, assuming perfectly rigid contact, are available on the topic.[1]

Mode-coupling instability is caused due to the coupling of several modes of vibration of one or more structures sliding along frictional constraint. Mode-coupling instability may or may not involve structural coupling. Hoffman and coworkers[4,5] consider mode-coupling instability in presence of structural coupling terms. Even though contact is modelled as compliant, the effects of contact parameters, such as contact stiffness and damping are not discussed. Duffour and Woodhouse[6,7] consider the transfer function approach to discuss the stability of sliding frictional contact at a single point. Discussion on the two-mode interaction is quite comprehensive and the effect of a third mode is also considered. The effects of contact compliance in normal and tangential directions are also addressed. However, the role of contact damping is missing in their discussion. Roles of normal, tangential, and angular mode coupling in friction-induced vibration have been addressed several times in reference.[8-10]

Besides mechanical systems with sliding components, sliding instabilities of the tectonic plates during earthquakes are also studied using the same class of models discussed above.[11,12] Other important classes of problems, similar to the problems of sliding instabilities, are discussed under the heading of the 'dynamics of multibody systems with unilateral constraints.'[13-15] These classes of problems deal with the dynamics of the contact bounce and the hopping phenomena of rigid or elastic multibody systems sliding along frictional boundaries. These studies find applications in robotic devices used for the sliding manipulation of objects.

Kinematic constraint instability is the central theme of the present article. Though in reference[1] this kind of instability is discussed in the context of rigid contact, it can be viewed as the special case of mode-coupling instability when compliance in the contact boundary allows elastic deformation. In order to throw light on some of the grey areas of the topic, the problem is framed in a rigorous physical and mathematical setup. Kinematic constraint instability is analysed from both rigid contact and compliant contact considerations with the objective of finding a point of convergence between the two formalisms. The minimal model of this kind of instability involves two structural modes. Even for this simple model, a complete picture of the stability characteristics is not available in literature. The present article tries to give a complete picture of the stability characteristics for two-mode interaction.

2. MATHEMATICAL MODEL AND STABILITY ANALYSIS

Friction induced self-excited instability is possible due to the mode-coupling effect. The minimal model explicating this effect involves two coupled structural modes of vibration.

The major objective of the present paper is to bring out the general effects of modal and contact parameters on the stability of two-mode sliding interaction at a point contact with constant coefficient of friction. Keeping the above objective in view, first the mathematical model of a specific system is considered. The mathematical model of this specific system helps one to reach a generalised mathematical model.

2.1. Mathematical Model of a Specific System

The mathematical model of an elastic element with tangential, normal and torsional compliance is depicted in Fig. 1. The elastic component is held, with the help of a preload, P_0, against a surface moving with velocity, v_s^*. The above model may be used to study the dynamics of a simple brake shoe and various other similar systems. Equations of motion of the system (for the situation when contact is active) are written as:

$$Mx'' + c_x x' + k_x x = F^*; \tag{1}$$

$$My'' + c_y y' + k_y y = P_0 - N^*; \tag{2}$$

$$J_\theta \theta'' + c_\theta \theta' + k_\theta \theta = P_0 L_2 + F^* H - N^* L, \tag{3}$$

where prime $(')$ denotes differentiation with respect to time, t. M and J_θ are mass and moment of inertia of the elastic element, respectively. $c_{x,y,\theta}$ and $k_{x,y,\theta}$ represent damping coefficients and stiffness in x, y, and θ directions, respectively. N^* and F^* represent normal and friction force, respectively. Normal contact deformation δ_c is expressed as:

$$\delta_c = y + L\theta. \tag{4}$$

For stable sliding contact, friction force is computed according to the Coulomb's model:

$$F^* = \mu N^*, \tag{5}$$

where μ is the coefficient of friction.

Non-dimensional equations of motion read as:

$$\ddot{X} + c_0 \dot{X} + X = \mu N; \tag{6}$$

$$\ddot{Y} + c_2 \dot{Y} + k_2 Y = P - N; \tag{7}$$

$$r^2\, \ddot{\theta} + c_1 \dot{\theta} + k_1 \theta = l_p P + (\mu h - l) N. \tag{8}$$

Non-dimensional parameters used in Eqs. (7)-(9) are defined below.

$$X = \frac{x}{x_0};\ Y = \frac{y}{x_0};\ x_0 = L;\ P = \frac{P_0}{x_0 M \omega_0^2};\ \omega_0 = \sqrt{\frac{k_x}{M}};$$

$$k_2 = \frac{k_y}{k_x};\ k_1 = \frac{k_\theta}{k_x};\ c_0 = \frac{c_x}{M\omega_0};\ c_2 = \frac{c_y}{M\omega_0};$$

$$c_1 = \frac{c_\theta}{M\omega_0 x_0^2};\ l_p = \frac{L_2}{x_0};\ h = \frac{H}{x_0};\ r^2 = \frac{J_\theta}{M x_0^2};\ v_s = \frac{v_s^*}{\omega_0 x_0};$$

$$K_c = \frac{k_c^*}{k_x};\ F = \frac{F^*}{M x_0 \omega_0^2};\ N = \frac{N^*}{M x_0 \omega_0^2}.$$

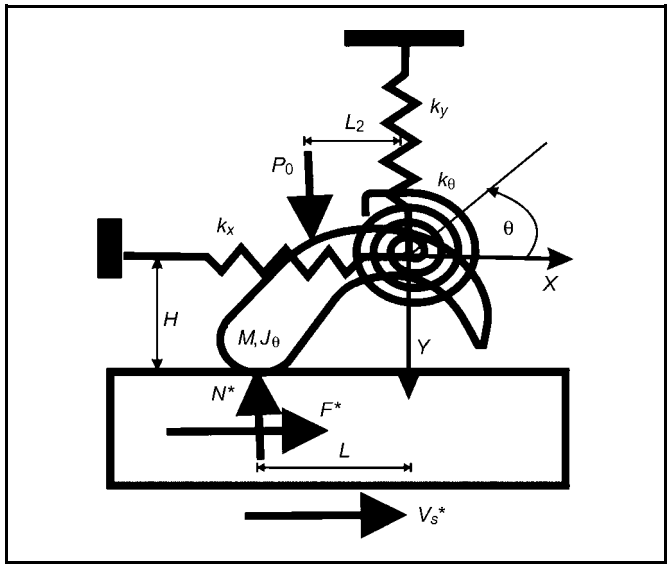

Figure 1. Mathematical model of a representative system.

In Eqs. (6)-(8), 'dot' denotes the differentiation with respect to the non-dimensional time $\tau = \omega_0 t$. For perfectly rigid contact condition, the normal contact deformation must be zero when one rewrites Eq. (4) in the following non-dimensional form:

$$Y + \theta = 0. \tag{9}$$

Before proceeding further, it may be noted that the tangential degree-of-freedom (X) has no effect on the stability of steady sliding. Therefore, only Eqs. (7) to (9) are relevant for ascertaining the stability of the system.

2.2. General Two-mode Interaction Model

For the general qualitative analysis of the stability of frictional sliding in the case of two-mode interaction, one may consider the following generalisation of Eqs. (7) and (8):

$$m_1 \ddot{X}_1 + c_1 \dot{X}_1 + k_1 X_1 + A_2 (X_1 - \beta_2 X_2) = f_1 N + \eta_1 P; \tag{10}$$

$$m_2 \ddot{X}_2 + c_2 \dot{X}_2 + k_2 X_2 + A_1 (X_2 - \beta_1 X_1) = f_2 N + \eta_2 P. \tag{11}$$

Here, X_i denotes the non-dimensional coordinate of the i-th degree-of-freedom and the time is normalised in the same fashion as in Eqs. (6)-(8). f_1 and f_2 are contact coupling factors and are, in general, functions of the coefficient of friction and other parameters of the system (geometry etc.). N and P represent non-dimensional normal load and external preload, respectively. η_1 and η_2 represent preload influence factors in mode 1 and 2, respectively. m_i, c_i, and k_i denote the i-th normalised modal mass, damping, and stiffness, respectively. Though the system shown in Fig. 1 does not involve any structural coupling terms between the modes of vibration, in a more general situation, structural coupling may be present. Therefore, structural coupling terms are also included in the generalised model. A_i and β_i are the structural coupling coefficients. It may be noted that the basis of the two structural modes involved is not a major concern; those may belong to the same component or to two different interacting components. Initially, structural coupling terms are considered absent, i.e., $A_1 = A_2 = 0$.

2.2.1. Rigid contact

As discussed earlier, the majority of early works consider rigid sliding contact. Under the assumption of rigid sliding contact, relative normal penetration at the contact point is zero. This is mathematically recast as a constraint equation. Though the constraint equation may be nonlinear in general, for small structural displacements, a linear constraint equation suffices for the stability analysis. Therefore, the following linear constraint equation is introduced:

$$\lambda_1 X_1 + \lambda_2 X_2 = 0. \tag{12}$$

In Eq. (12), λ_1 and λ_2 represent constraint coefficients. One may note that the constraint Eq. (12) is the generalisation of Eq. (9). Using Eq. (12) in Eqs. (10) and (11) and eliminating N, one finally obtains:

$$M_e \ddot{X}_2 + C_e \dot{X}_2 + K_e X_2 = (\eta_1 f_2 - \eta_2 f_1)P, \tag{13}$$

where

$$M_e = -m_1 \lambda f_2 \left\{1 - \frac{m_2}{m_1}\Delta\right\};\ C_e = -c_1 \lambda f_2 \left\{1 - \frac{c_2}{c_1}\Delta\right\};$$

$$K_e = -k_1 \lambda f_2 \left\{1 - \frac{k_2}{k_1}\Delta\right\},$$

with $\lambda = \lambda_2/\lambda_1, \Delta = -f_1/\lambda f_2$.

From Eq. (13), it is inferred that the steady sliding state is stable if, and only if, M_e, C_e, and K_e bear the same sign. Thus, steady sliding becomes unstable in more than one way. Further discussions on this are deferred until section 2.2.4. At this point, validity of rigid contact assumption is questioned. In what follows, the problem is analysed in a more rigorous and realistic setup considering the contact point as compliant and the normal penetration at the contact point as non-zero. Rigidity of the contact point may be approached in the limit of high contact stiffness.

2.2.2. Rigid contact as the limiting case of compliant contact

According to the Kelvin-Voigt viscoelastic model of compliant contact, normal force of interaction is expressed as:

$$N = K_c(\lambda_1 X_1 + \lambda_2 X_2) + D_c(\lambda_1 \dot{X}_1 + \lambda_2 \dot{X}_2), \tag{14}$$

where K_c and D_c represent normalised contact stiffness and damping constant, respectively. For compliant contact condition, contact deformation is small but non-zero, even for reasonably high contact stiffness. Therefore, one rewrites Eq. (12) as:

$$\lambda_1 X_1 + \lambda_2 X_2 = \varepsilon Z. \tag{15}$$

Now the normal contact force is expressed as:

$$N = \frac{1}{\varepsilon}\varepsilon Z + \frac{d_c}{\sqrt{\varepsilon}}\varepsilon \dot{Z}, \tag{16}$$

Where $\varepsilon = 1/K_c \ll 1$ and $d_c = D_c\sqrt{\varepsilon}$. Z is the conservative part (i.e., elastic component) of the normal force N. Introducing Eqs. (15) and (16) in Eqs. (10) and (11), one obtains

$$\varepsilon m_1 \ddot{Z} + \left(\delta_4 - \frac{d_c \delta_0}{\sqrt{\varepsilon}}\right)\varepsilon \dot{Z} + \left(\delta_3 - \frac{\delta_0}{\varepsilon}\right)\varepsilon Z + \delta_1 \dot{X}_2 + \delta_2 X_2 = \delta_5, \tag{17}$$

where

$$\delta_0 = \frac{\lambda_2 m_1}{m_2} f_2 + \lambda_1 f_1;\ \delta_1 = \frac{\lambda_2 m_1}{m_2} c_2 - \lambda_2 c_1;$$

$$\delta_2 = \frac{\lambda_2 m_1}{m_2} k_2 - \lambda_2 k_1;\ \delta_3 = k_1;\ \delta_4 = c_1;$$

$$\delta_5 = \left(\frac{\lambda_2 m_1}{m_2}\eta_2 + \eta_1 \lambda_1\right)P.$$

Equation (19) assumes the standard form of singular perturbation[16] problem if the following two restricted conditions are satisfied:

$$\delta_4 - \frac{d_c \delta_0}{\sqrt{\varepsilon}} \sim O\left(\varepsilon^{-\frac{1}{2}}\right), \tag{18}$$

and

$$\delta_3 - \frac{\delta_0}{\varepsilon} \sim O(\varepsilon^{-1}). \tag{19}$$

Putting $\varepsilon = 0$ (that corresponds to a perfectly rigid constraint) in Eq. (17), the slow manifold (which describes the slow dynamics i.e., dynamics captured in the natural time scale of the system) of the system is obtained as follows:

$$Z = v_0 + v_1 X_2 + v_2 \dot{X}_2, \tag{20}$$

where

$$v_0 = -\frac{\delta_5}{\delta_0};\quad v_1 = \frac{\delta_2}{\delta_0};\quad v_2 = \frac{\delta_1}{\delta_0}.$$

Obviously, the slow manifold represents the solution consistent with the rigid contact condition. Following co-ordinate and time transformations are applied to Eq. (19):

$$\zeta = Z - v_0 - v_1 X_2 - v_2 \dot{X}_2 \tag{21}$$

and

$$\tau_f = \frac{\tau}{\sqrt{\varepsilon}}, \tag{22}$$

where ζ represents the deviation Z from the slow manifold and τ_f represents a rescaled time which will be used to capture the fast dynamics of the deviation ζ. Fast dynamics of the deviation ζ from the slow manifold is given by the Tikhonov's Boundary Layer equation obtained below:

$$m_1 \frac{d^2\zeta}{d\tau_f^2} - \delta_0 d_c \frac{d\zeta}{d\tau_f} - \delta_0 \zeta = 0. \tag{23}$$

The equilibrium $\zeta = 0$ of Eq. (23) is uniformly asymptotically stable for $\delta_0 < 0$. According to the Tikhonov's Theorem, stability of $\zeta = 0$ implies that the slow manifold, governed by Eq. (20), represents an approximate solution (accurate up to $O(\varepsilon)$) of Eq. (17). Thus, the assumption of the rigid constraint is valid only for $\delta_0 < 0$. However, in case of unstable boundary layer, one has to consider the effect of contact compliance.

2.2.3. LCP formulation and the Painleve paradox

The Linear Complementary Problem (LCP)[17] of the rigid sliding contact is formulated considering the contact deformation (εZ) and the contact deformation rate ($\varepsilon \dot{Z}$) as zero. Thus, one deals with only the conservative part of the normal load, i.e., $N = Z$. Denoting the normal contact acceleration $\varepsilon \ddot{Z}$ as a, the LCP is formulated from Eq. (17) as follows:

$$a = AN + b, \tag{24}$$

where

$$A = \frac{\delta_0}{m_1}; \quad b = \frac{\delta_5 - \delta_1 \dot{X}_2 - \delta_2 X_2}{m_1}.$$

For maintaining the contact, the following conditions must be satisfied

$$aN = 0 \ \forall \ a \geq 0, N \geq 0. \tag{25}$$

Possible solutions of the LCP Eq. (24) and the corresponding stability conditions of the boundary layer Eq. (23) are listed in Table 1. For $\delta_0 \geq 0$, there exist three possibilities: 1) non-contact solution, 2) non-unique solutions, or 3) no solution at all. Non-existence and non-uniqueness of the solutions of the contact sliding problems is known as the Painleve paradox in the literature. However, the condition of the Painleve paradox $(\delta_0 \geq 0)$ coincides with the boundary of invalidity of the rigid contact assumption, which forms the basis of the Painleve paradox. As $\delta_0 \geq 0$ condition warrants the use of compliant contact model, the Painleve paradox is resolved under the compliant contact assumption. Even though the Painleve paradox is not the central theme of this article, certain instability phenomena[13] are strongly connected to it. This is discussed elsewhere in the paper. Now the discussion again reverts to the stability of sliding.

Table 1. The symbol p denotes Painleve paradox.

Conditions	LCP solutions for rigid sliding contact	Stability of boundary layer
$A < 0, b < 0$	$N = 0, a = b$: no contact	Stable
$A < 0, b = 0$	$N = 0, a = 0$: no contact	Stable
$A < 0, b > 0$	$N = -b/A, a = 0$: contact	Stable
$A > 0, b < 0$	$N = 0, a = b$: no contact	Stable
	$N = -b/A, a = 0$: contact	Unstable
$A > 0, b = 0$	$N = 0, a = 0$: no contact	Stable
$A > 0, b > 0$ (p)	No solution	N/A
$A = 0, b < 0$	$N = 0, a = b$: no contact	Stable
$A = 0, b = 0$ (p)	Infinite number of solutions	
$A = 0, b > 0$ (p)	No solution	N/A

2.2.4. Stability analysis for rigid contact

One may note that

$$M_e = -\frac{m_2 \delta_0}{\lambda_1}. \tag{26}$$

One rewrites Eq. (13) as

$$-m_2 \delta_0 \ddot{X}_2 + \lambda_1 C_e \dot{X}_2 + \lambda_1 K_e X_2 = \lambda_1 (\eta_1 f_2 - \eta_2 f_1) P. \tag{27}$$

As the condition for a well-defined and unique rigid contact is $\delta_0 < 0$, sliding becomes unstable when $\lambda_1 C_e$ and/or $\lambda_1 K_e$ are negative. From Eq. (13), the following important parameters that influence the stability, are identified: $K_r = k_2/k_1$, $C_r = c_2/c_1$, $m_r = m_2/m_1$, and $\Delta = -f_1/\lambda f_2$. Though it is not possible to ascertain the sign of the parameters in general, one may rearrange the mathematical model of a particular system to satisfy the following conditions:

$$\chi = \lambda_2 f_2 < 0, \tag{28}$$

and

$$\Delta > 0. \tag{29}$$

This signifies that the numbering of the modes may be done to satisfy the above two conditions. Now the stability boundary is delineated in Δ vs. c_r plane. Depending upon the other parameter values, two cases arise and these are shown in Figs. 2(a) and (b).

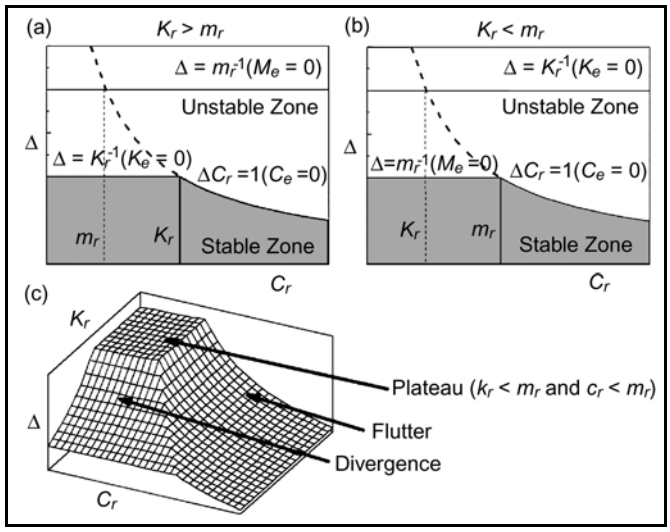

Figure 2. Stability plots for steady perfectly rigid contact sliding.

Case I: $K_r > m_r$ (Fig. 2(a)). For the higher ratios of modal damping C_r $(> K_r)$, stability boundary is defined by the hyperbolic line $\Delta C_r = 1$, which corresponds to $C_e = 0$. Hopf bifurcation leading to flutter type instability of the steady sliding condition takes place across this line. However, for lower values of C_r, stability is lost across the line $\Delta = 1/K_r$, which runs parallel to the C_r axis and corresponds to $K_e = 0$. The associated motion leads to divergence type instability.

Case II: $K_r < m_r$ (Fig. 2(b)). Similar to the Case I, stability boundary for higher modal damping ratio $(C_r > m_r)$ is given by the hyperbolic line $\Delta C_r = 1$. Across this line, stability is lost by the Hopf bifurcation leading to flutter. However, when $C_r < m_r$, the condition $\delta_0 = 0$ or $M_e = 0$ is reached on the $\Delta = 1/m_r$ line, which is below the hyperbolic line. One must understand that on and beyond this boundary, the rigid contact assumption fails. A more complete description of the system in this parameter zone warrants the consideration of compliant contact model, where rigidity of the contact may be approached in the limit, i.e., by putting a high numerical value of the contact stiffness. However, if one still sticks to the rigidity assumption, the conditions of the Painleve paradox (as discussed in section 2.2.3) may be satisfied. The associated bifurcation across this boundary and the corresponding instability is termed as 'the bifurcation induced by the Painleve paradox' in some recent reference.[13] However, characteristics of this kind of bifurcation should be studied using a complaint contact model.

Similar stability boundary is obtained by presenting the plot in Δ vs. K_r plane where C_r and K_r exchange the respective roles. A complete picture of the stability zone is depicted in Fig. 2(c), where the stability surface is generated by plotting the critical value of Δ with respect to C_r and K_r. The region below the surface corresponds to stable sliding. Three distinct zones of the stability surface are apparent from Fig. 2(c) and each zone represents a distinct instability. In the region of higher K_r $(> m_r)$ and lower C_r $(< K_r)$, stability is lost by divergence, whereas flutter is observed for higher values of

C_r ($> \max(K_r, m_r)$). However, the stability surface looks like a flat plateau for lower values of C_r and K_r (both less than m_r). On and above the entire flat plateau, either there is loss of contact or the conditions of the Painleve paradox are satisfied. In the context of rigid contact analysis, this surface coincides with the Painleve paradox induced bifurcation.[13] However, as the rigid contact assumption is not valid on and above this flat plateau, stability analysis based on a more realistic compliant contact model is required for this region and the rigidity of contact is to be simulated as the limiting condition (for very high value of contact stiffness) of the complaint contact model.

The singular perturbation analysis presented in section 2.2.2 throws significant light on the possible instability mechanism. The boundary layer equation (Eq. (23)) gives a linear description of the fast local dynamics of an arbitrary perturbation ζ imposed on the slow manifold (steady normal load corresponding to steady sliding) and this dynamics case is described on a rescaled time (fast), τ_f. Therefore, when the equilibrium of the boundary layer equation becomes unstable just on the flat plateau, perturbation is expected to drift away very fast from the steady state normal load, and consequently steady sliding becomes unstable. Under such circumstances, one cannot physically reduce the order of the model, because the normal load fluctuation is governed by another independent degree-of-freedom (faster compared to the structural degrees-of-freedom), which may be termed hereafter as the contact degree-of-freedom. One must discern this instability as different from ordinary divergence or flutter where instability is not strongly governed by the contact degree-of-freedom. It is enlightening to note that under the jurisdiction of perfectly rigid contact assumption, the stable slow manifold (Eq. (20)) describes the conservative part of the normal force and thus, the dissipative part of the normal force is negligibly small. Therefore, normal contact force either remains steady (for stable sliding) or varies slowly and/or oscillates with low frequency (for unstable sliding) for the parameter values that promote the perfectly rigid contact assumption.

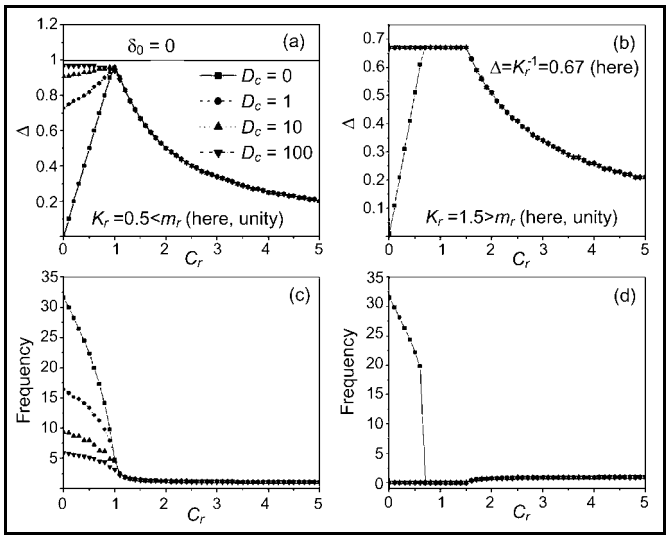

Figure 3. Variation of Stability and frequency plots with contact damping for linear compliant contact, $K_c = 1000$. (a) and (c) $K_r = 0.5$; (b) and (d) $K_r = 1.5$.

2.2.5. Stability analysis for compliant contact

From the discussions made in the preceding sections, it is apparent that the rigid contact model is not uniformly valid in the entire parameter space, particularly when $\delta_0 < 0$. In this section, stability of sliding is analysed using compliant contact, where the normal load is expressed as given in Eq. (14). Using Eq. (14), Eqs. (10) and (11) are rewritten as:

$$m_1 \ddot{X}_1 + (c_1 - \lambda_1 f_1 D_c)\dot{X}_1 + (k_1 - \lambda_1 f_1 K_c)X_1 - f_1 \lambda_2 K_c X_2 - f_1 \lambda_2 D_c \dot{X}_2 = \eta_1 P, \quad (30)$$

$$m_2 \ddot{X}_2 + (c_2 - \lambda_2 f_2 D_c)\dot{X}_2 + (k_2 - \lambda_2 f_2 K_c)X_2 - f_2 \lambda_1 K_c X_1 - f_2 \lambda_1 D_c \dot{X}_1 = \eta_2 P. \quad (31)$$

Now the stability of sliding contact is determined by the eigenvalue analysis of the following Jacobian matrix of the flow of Eqs. (30) and (31):

$$J = \begin{bmatrix} 0 & 1 & 0 & 0 \\ \frac{\lambda_1 f_1 K_c - k_1}{m_1} & \frac{\lambda_1 f_1 D_c - c_1}{m_1} & \frac{f_1 \lambda_2 K_c}{m_1} & \frac{f_1 \lambda_2 D_c}{m_1} \\ 0 & 0 & 0 & 1 \\ \frac{f_2 \lambda_1 K_c}{m_2} & \frac{f_2 \lambda_1 D_c}{m_2} & \frac{\lambda_2 f_2 K_c - k_2}{m_2} & \frac{\lambda_2 f_2 D_c - c_2}{m_2} \end{bmatrix}. \quad (32)$$

Sliding is stable if, and only if, all the eigenvalues of J have negative real parts. Now one can easily construct the stability surfaces by plotting critical values of Δ with respect to C_r and K_r. The effect of normal contact compliance on the stability of sliding is discussed with respect to the reference stability surface shown in Fig. 2(c) that is obtained for the perfectly rigid contact. To avoid unwieldy algebra, a closed form expression the stability surface for compliant contact is not attempted here. Specific numerical examples are taken to discuss the effects of normal contact compliance on the stability surface. Without losing any generality, the following parameter values are chosen for subsequent discussions:

$$m_1 = m_2 = 1.0;\ \lambda_1 = \lambda_2 = 1.0;\ c_1 = 0.1;\ k_1 = 1;\ f_2 = -1.$$

Now f_1, k_2, and c_2 are varied to satisfy the conditions Eqs. (28) and (29). With the objective of simulating rigid contact condition, the contact stiffness parameter, K_c, is chosen to be a few orders higher in magnitude than the system stiffness parameters, k_1 and k_2. Stability threshold lines and the corresponding frequencies of instability are plotted in Fig. 3. As before, two separate cases arise.

Case I: $K_r = 0.5 < m_r$ (Figs. 3(a) and (c)). It is evident from Figs. 3(a) and (c) that the stability threshold value is less than that corresponding to the rigid contact condition for $C_r < m_r$ (here, unity). With the increasing value of D_c, the stability boundary gradually approaches the limiting value defined by $\Delta = 1/m_r$ (equivalent to $\delta_0 = 0$) line corresponding to the rigid contact condition. Under these circumstances, stability is always lost by high frequency flutter. Therefore, in these range of parameter values, the stability characteristics of the compliant sliding contact are substantially different from that for rigid contact condition except for large value of contact damping. However, for $C_r > m_r$, stability is lost due to low frequency flutter. In this region, contact damping does not have any appreciable effect on the stability threshold.

Therefore, resemblance of the stability characteristics with the rigid contact condition is observed in the higher range of values of C_r.

Case II: $K_r = 1.5 > m_r$ (Figs. 3(b) and (d)). Low frequency flutter is observed for higher values of C_r ($> K_r = 1.5$here). The stability threshold remains independent of contact damping. For lower values of C_r ($< K_r$), the stability thresholds, as well as the type of instability, strongly depend on contact damping. With low value of D_c, the stability threshold is below the corresponding value observed in case of rigid contact, i.e., $\Delta = 1/K_r$ ($= 0.67$ here) line. In addition, the stability is not lost due to divergence in the entire lower range of values of C_r ($< K_r$). However, for large contact damping, the stability threshold and the type of instability (divergence) in the lower range of values of C_r ($< K_r$) match perfectly with that obtained in case of rigid contact sliding.

A complete, as well as qualitatively generic, description of the stability characteristics over the entire parameter space is illustrated in Fig. 4. Similar to the case of rigid contact condition, three distinct stability zones exist also in the case of compliant contact. However, the plateau region is only observed in the limit of high value of contact damping $\sim O(\sqrt{K_c})$. For relatively lower values of contact damping, the stability threshold surface is a slanted surface (which lies below the plateau) in the region of low C_r. However, with the increasing value of contact damping, the slanted surface approaches the shape of flat plateau. For higher values of contact damping, the stability zone expands in the region of low C_r and K_r. Evidently, contact damping (> 0) has a minimal or no effect on the stability zone for higher values of K_r and C_r.

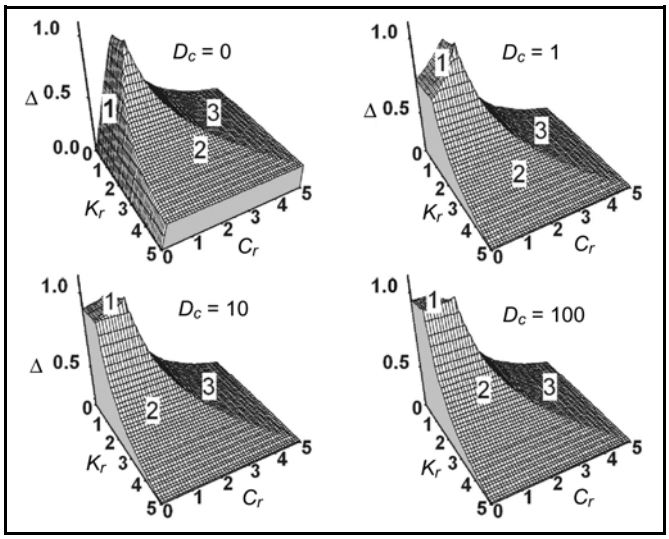

Figure 4. Stability surface plots for linear compliant contact model, $K_c = 1000$.

In Fig. 5, imaginary parts of the marginally unstable eigenvalues are plotted against C_r and K_r. Imaginary parts of the marginally unstable eigenvalues signify the frequency of perturbation growth. Zero frequency corresponds to divergence. Depending upon the frequency of instability, one demarcates three different regions of the stability surfaces depicted in Fig. 4. The regions marked as 1, correspond to high frequency flutter. It is not difficult to envisage that the high frequency flutter is associated with an extremely active contact phenomenon. The regions marked as 2 and 3, correspond to divergence and low frequency flutter, respectively. From the above observations, one may conclude that the rigid contact assumption may not be uniformly valid over the entire parameter space. The stability zone computed from the rigid contact assumption deviates substantially from that obtained from the compliant contact model when both C_r and K_r assumes low values ($< m_r$). However, for higher values of both C_r and K_r, the rigid contact condition turns out to be a valid assumption.

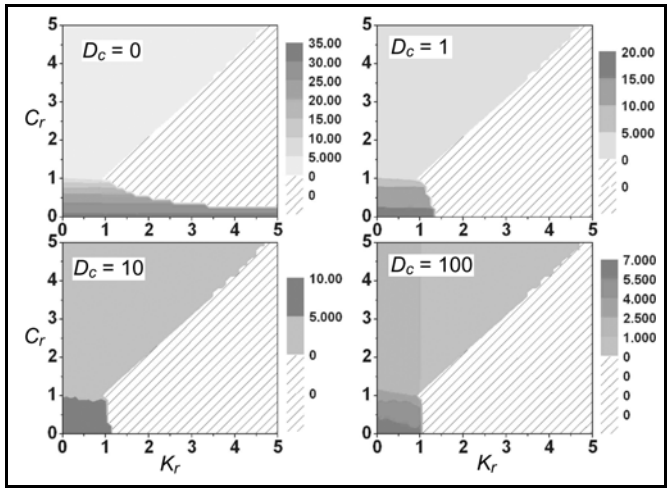

Figure 5. Frequency maps for linear compliant contact model, $K_c = 1000$.

It is fairly interesting and counterintuitive to note that when contact damping is zero, the flat plateau (the characteristic part of the stability surface obtained from the perfectly rigid contact formalism) cannot be produced in the limiting condition of compliant contact model even for a very large value of contact stiffness. However, the flat plateau consistently appears for large values ($O(\sqrt{K_c})$) of contact damping. Then what is the point of convergence between the perfectly rigid contact formalism and the compliant contact doctrine? The question of non-convergence is of course relevant for only a particular parameter region, i.e., the region where the flat plateau exists. The above analysis and results suggests that the compliant contact model can simulate conditions similar to the perfectly rigid contact only for high contact stiffness and damping. However, so long as contact is maintained, the perfectly rigid contact model does not regard any form of contact damping. Damping in the form of coefficient of restitution becomes relevant only after contact separates due to instability followed by reengagement through impact. Thus, for studying sliding stability, one naturally tends to simulate rigid contact condition by using high value of contact stiffness and zero contact damping in the compliant contact model. However, the above results clearly indicate that perfectly rigid contact conditions are not obtained for zero contact damping. According to the singular perturbation analysis, the compliant contact model does not approach the rigid contact condition in unconditional and stable fashion for higher values of contact damping in the order of $O(\sqrt{K_c})$. Even though similar results are not available for zero contact damping (One requires high damping in the first mode to continue with the singular perturbation analysis. Such a situation, being unrealistic, is not pursued here), it is reasonable to believe that the perfectly rigid contact condition is also not

approached in a stable fashion from a compliant contact model with zero contact damping. Results of the compliant contact model confirm this belief.

In a number of practical situations, the contact surface may be sufficiently compliant such that the contact stiffness is of the same order of magnitude as the structural stiffness parameters. Stability surfaces are plotted in Fig. 6 for low values of contact stiffness and different values of contact damping. As illustrated in Fig. 6, the flat plateau appears in the stability surface for a large value of contact damping. From Fig. 7, one observes that high frequency flutter is possible for low C_r and K_r. It is also noted that the divergence region (hatched region) becomes substantially constricted for higher contact damping as compared to what is observed in the case of stiff contact.

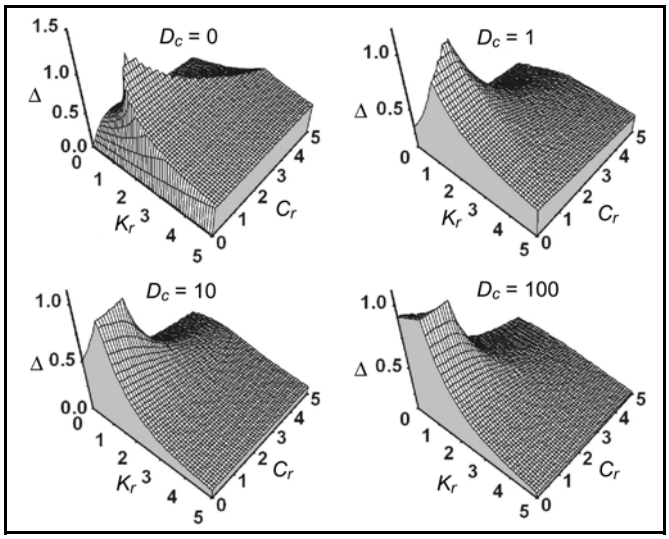

Figure 6. Stability surface plots for $K_c = 5$.

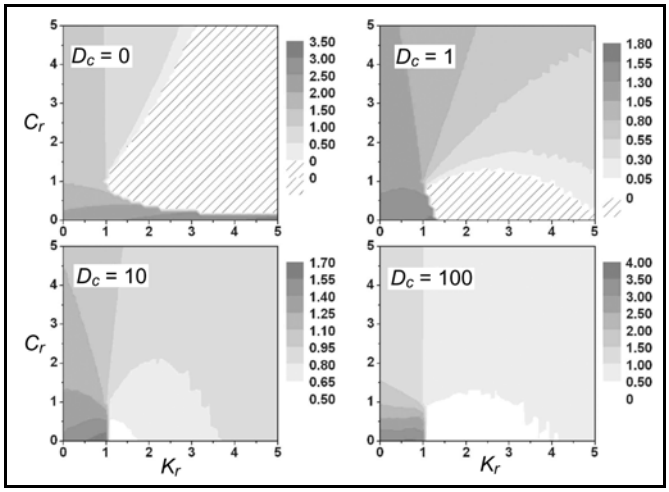

Figure 7. Frequency map for $K_c = 5$.

3. STABILITY ANALYSIS FOR NONLINEAR CONTACT MODEL

In the foregoing analysis, the simplified Kelvin-Voigt type linear model is considered for the computation of contact force. The major deficiency of a linear model is that it may give rise to negative contact force during contact separation, which is a nonphysical situation. This is ascribed to the presence of linear dissipative term in the contact model. This unrealistic situation is circumvented if normal contact force is computed according to the Hunt-Crossley model,[18] which incorporates nonlinear elastic and dissipative terms as follows:

$$N = K_c(\delta_c^{\beta} + \frac{3}{2}\alpha\delta_c^{\beta}\dot{\delta}_c)\,. \tag{33}$$

where δ_c and $\dot{\delta}_c$ are the contact deformation and the deformation rate, respectively and are given by:

$$\delta_c = \lambda_1 X_1 + \lambda_2 X_2\,; \quad \dot{\delta}_c = \lambda_1 \dot{X}_1 + \lambda_2 \dot{X}_2\,. \tag{34}$$

α and β are the two parameters of the model and values of these parameters depend on the material and geometry of the contact. β models the non-linearity of the contact spring and α determines the level of contact damping. Stability analysis can be carried out using Eqs. (10), (11) and (33) in a manner similar to that explained in section 2.1.5. For stability analysis, one must find out the equilibrium configuration corresponding to steady sliding condition as given below

$$X_{eq} = \{X_1 = x_{10}, \dot{X}_1 = 0, X_2 = x_{20}, \dot{X}_2 = 0\}^T, \tag{35}$$

where x_{10} and x_{20} are obtained as

$$x_{10} = \frac{f_1 K_c \Delta_0^{\beta} + \eta_1 P}{k_1}; \quad x_{20} = \frac{f_2 K_c \Delta_0^{\beta} + \eta_2 P}{k_2}, \tag{36}$$

where Δ_0 is the solution of the following equation:

$$a_0 \Delta^{\beta} - \Delta + a_1 = 0\,, \tag{37}$$

with

$$a_0 = K_c\left(\frac{f_1\lambda_1}{k_1} + \frac{f_2\lambda_2}{k_2}\right); \quad a_1 = P\left(\frac{\lambda_1\eta_1}{k_1} + \frac{\lambda_2\eta_2}{k_2}\right). \tag{38}$$

Now, the stability of steady sliding is determined by the eigenvalues of the following Jacobian matrix computed at the equilibrium X_{eq}:

$$J = \begin{bmatrix} 0 & 1 & 0 & 0 \\ \frac{-k_1 + f_1 D_1}{m_1} & \frac{-c_1 + f_1 D_1^*}{m_1} & \frac{f_1 D_2}{m_1} & \frac{f_1 D_2^*}{m_1} \\ 0 & 0 & 0 & 1 \\ \frac{-k_2 + f_2 D_1}{m_2} & \frac{-c_2 + f_2 D_1^*}{m_2} & \frac{f_2 D_2}{m_2} & \frac{f_2 D_2^*}{m_2} \end{bmatrix}; \tag{39}$$

$$D_i = \left.\frac{\partial N}{\partial X_i}\right|_{X_{eq}} = K_c \beta \lambda_i \Delta_0^{\beta-1}, \quad \text{for } i = 1, 2\,, \tag{40}$$

and

$$D_i^* = \left.\frac{\partial N}{\partial \dot{X}_i}\right|_{X_{eq}} = \frac{3}{2} K_c \alpha \lambda_i \Delta_0^{\beta}, \quad \text{for } i = 1, 2\,. \tag{41}$$

More often, β is close to unity,[19] but the value may vary widely depending upon the geometry and material. For example, in case of non-conformal contact, the Hertzian contact theory suggests $\beta = 1.5$. For subsequent analysis, the value of β is taken as unity. Considering the focus of the present analysis being on the qualitative aspects of the stability characteristics, such a choice does not defeat the purpose. Moreover, it has been noted that contact damping plays a vital role in determining the shape of the stability surface. Therefore,

the effect of the dissipative part of the contact force is explored in the present section. The chosen value of β renders the dissipative part of the contact force nonlinear, keeping the conservative part linear and intact.

Stability surfaces and the corresponding frequency maps are depicted in Figs. 8 and 9, respectively. Three regions of the stability surfaces are identified as before and these are marked as 1, 2, and 3. Regions marked as 1 and 3 correspond to high frequency and low frequency flutter, respectively. One observes that for large values of the contact damping parameter α, the flat plateau appears in the region (region 1) of low values of K_r and C_r. However, the characteristics of the stability regions marked as 2 are qualitatively different from that observed for linear contact model, particularly for the low level of contact damping. In the case of the linear contact model, region 2 corresponds to divergence. Whereas for the nonlinear contact model, the surfaces marked as 2 do not correspond solely to divergence; for low values of contact damping, a good portion of this surface correspond to high or low frequency flutter. However, when contact damping is substantial, the entire region of the surface represents divergence, similar to what has been observed previously for linear contact model.

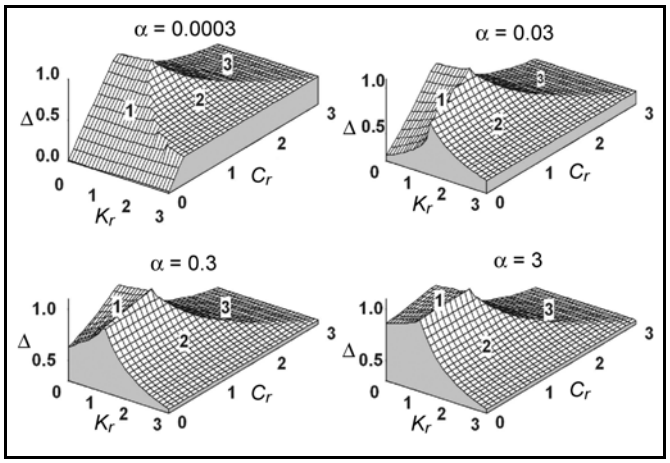

Figure 8. Stability plot for nonlinear contact model, $K_c = 1000$.

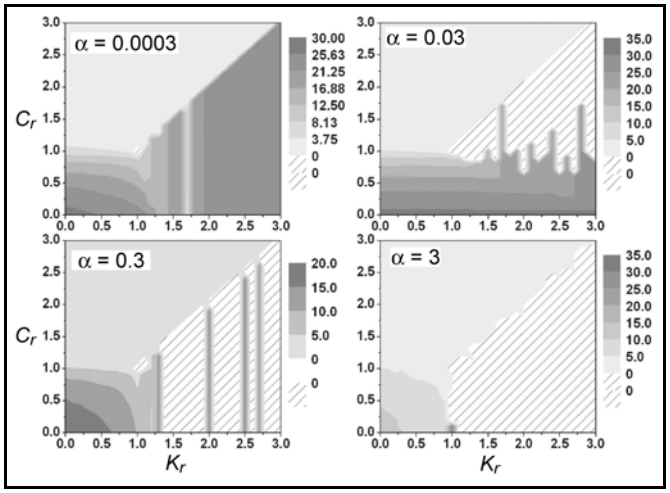

Figure 9. Frequency map for nonlinear contact model, $K_c = 1000$.

One may note the interesting fact that the linear contact model does not bring out the effect of preload parameters, η_1, η_2, and P on the stability surface. However, it may be observed from Eqs. (35)-(41) that the nonlinear contact model reveals the influence of preload parameters on the stability of sliding. From the stability surface plots and the frequency maps (results are not presented due to the lack of space) one may conclude that the increasing level of preload has a more or less similar qualitative effect as caused by the increasing level of contact damping. Similar effects are also revealed if, instead of P, any one or both of the other preload factors η_1 and η_2 are increased, keeping other parameters fixed.

Effects of the structural coupling terms A_1 and A_2 on the stability of sliding are also studied. Stability surfaces and the corresponding frequency maps are plotted against C_r and K_r for different values of A_1 and A_2 (results are not presented). It is observed that for the increasing value of A_1, with A_2 fixed at a certain value, the plots (both the stability and frequency plots) undergo a shift towards the lower range of K_r. The shift is just towards the opposite direction in case of the increasing value of A_2.

4. AN EXAMPLE SYSTEM

Here, the example system considered in section 2.1 is analysed in light of the foregoing discussions. Eqs. (6)-(8) are numerically simulated. Numerical computation of the friction force during stick-slip or slip-stick contact transition is a very difficult process. Because of the discontinuity at zero velocity, the Coulomb's model is not numerically efficient. This is circumvented in a large number of regularised models proposed in literature. Here, the following model proposed by Martins and Oden[10] is considered

$$F = \begin{cases} -\left(\dfrac{\mu N}{\varepsilon_c}\right)(v_s - \dot{X} - h\dot{\theta}), & \text{if } |v_s - \dot{X} - h\dot{\theta}| \leqslant \varepsilon_c\,; \\ -\mu N \operatorname{sgn}(v_s - \dot{X} - h\dot{\theta}), & \text{if } |v_s - \dot{X} - h\dot{\theta}| > \varepsilon_c\,. \end{cases} \tag{42}$$

In the above model of friction, ε_c represents a small non-dimensional quantity of the order of magnitude 10^{-4}. Normal contact force N is computed according to the Hunt-Crossley model given by Eq. (33). Now comparing Eqs. (7) and (8) with Eqs. (10) and (11), respectively one notes that

$$X_1 = \theta;\ m_1 = r^2;\ P = 1;\ \eta_1 = l_p;\ f_1 = \mu h - 1;$$

$$X_2 = Y;\ m_2 = 1;\ \eta_2 = 1;\ f_2 = -1;\ \lambda_1 = 1;\ \lambda_2 = 1.$$

Therefore, $\Delta = (\mu h - 1) > 0$ for $\mu h > 1$ and $\chi = -1 < 0$. Thus, the conditions Eqs. (28) and (29) discussed in section 2.2.4 are satisfied for $\mu h > 1$. The following non-dimensional parameter values are considered for the subsequent discussions: $k_1 = 1.0$, $c_1 = 0.1$, $r = 1.0$, $l_p = 1.0$, $K_c = 10^3$, $\xi_c = 1.5\alpha x_0 \omega_0 = 10^{-5}$, $\mu = 0.5$. Other parameter values are varied as and when required. The stability characteristics of the system are depicted in Fig. 10 where stability threshold lines and the corresponding frequencies of unstable growth (imaginary parts of the unstable eigenvalues) are plotted with respect C_r for two different values of k_2. From these plots, one easily observes the existence of the high frequency, low frequency flutter lines, and the divergence threshold lines. In order to reveal the nature of the normal load variation across the high frequency and low frequency flutter lines, equation of motion are numerically simulated in MATLAB. Time history of the normal load variation at the two stability boundaries are plotted in Fig. 11. One observes that for $c_2 = 0.3$,

normal load oscillates with low frequency at the stability threshold and after the initial growth is over, the normal load continues to oscillate with low frequency without any loss of contact (not shown). Whereas for $c_2 = 0.05$, normal load varies with very high frequency at the point of instability and the high frequency transient ultimately leads to intermittent contact bounce and reengagement through impact.

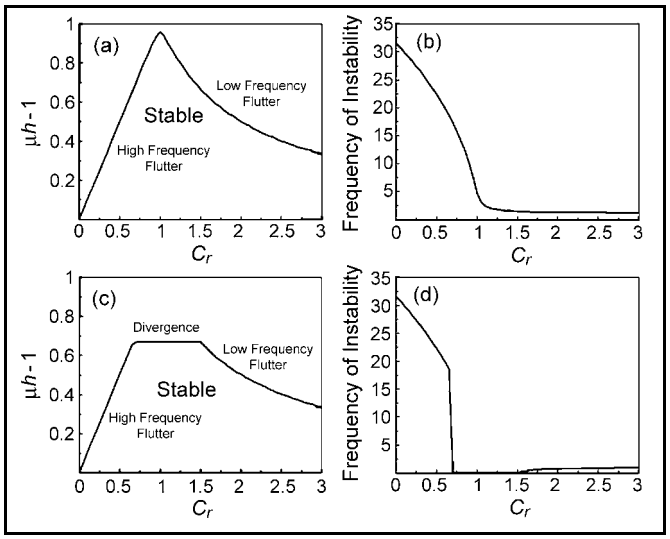

Figure 10. Stability and frequency plot for the example system. (a) and (b) $k_2 = 0.5$; (c) and (d) $k_2 = 1.5$.

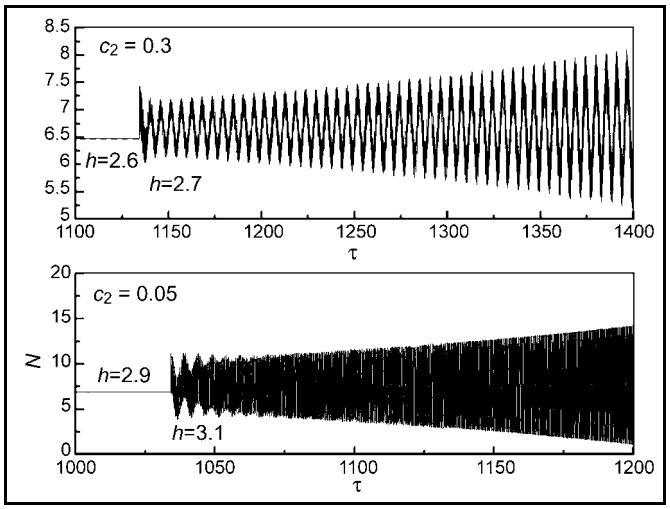

Figure 11. Numerically simulated time history of normal force. $c_1 = 0.1$, $k_2 = 0.5$, $k_1 = 1$, $l_p = 1$, $\mu = 0.5$, $v_s = 10$, $K_c = 1000$, $\xi_c = 10^{-5}$.

5. CONCLUSIONS

Friction induced sliding instabilities due to the interaction of two structural modes of vibration is the central theme of the present paper. A general mathematical model of sliding elastic systems represented by two interacting modes of vibration is considered to explore the effects of various parameters on the nature of instability. Both rigid and compliant contact conditions are analysed and compared. Several important conclusions are drawn from the discussions made in the article and these are as follows:

1. In a two-mode interaction model, sliding friction contact causes three types of instabilities namely, low-frequency flutter, high-frequency flutter, and divergence. The dynamics involved in high-frequency flutter is interesting and has received special attention in the paper. It is shown that this particular type of instability cannot be explained in the rigid contact formalisms. One requires a compliant contact model to explain the exact nature of the instability. It is also observed that the condition of the Painleve paradox induced bifurcation in the rigid contact model coincides with the high-frequency flutter boundary. Though numerical evidences of high-frequency instability exist in references,[11,12] rigorous mathematical analysis was missing so far.
2. It is shown that, except in a particular parameter region, rigid contact assumption is valid in terms of the shape, size, and characteristics of the stability surface. However, there exists a parameter region where the results of the compliant contact model do not converge to that obtained from the rigid contact model. This result is known in the context of rigid body interaction.[15] However, to the best of the author's knowledge, the results are first extended for interacting bodies with elastic degrees-of-freedom in this article.
3. The most interesting finding of the article is that perfectly rigid contact conditions can be simulated from the compliant contact formalism only for high values of contact stiffness (K_c) with high contact damping in the order of $O(\sqrt{K_c})$. However, a perfectly rigid contact condition is not equivalent to a compliant contact condition with extremely high contact stiffness, but zero contact damping. Of course, this conclusion holds good only in a specific parameter region. This is a new finding of the present article.
4. Dissipative part of the contact force plays the most dominating role in ascertaining the stability of sliding, as well as differentiating between the perfectly rigid contact model and the compliant contact model. It is observed that a disproportionate distribution of damping among different modes is in general detrimental and this conforms to the previous findings.[4,5] However, for higher values of contact damping, the above conclusion does not hold true in a particular parameter region. This is also a new finding of the present article.

Future work should consider the analysis of multi-mode interaction. The effect of contact damping on distributed contact must also be addressed.

REFERENCES

[1] Ibrahim, R. A. Friction-induced vibration, chatter, squeal and chaos II: dynamics and modeling, *ASME Applied Mechanics Reviews*, **47**, 227-253, (1994).

[2] Wallaschek, J., Hach, K. H., Stolz, U., and Mody P. A survey of the present state of friction modelling in the analytical and numerical investigation of brake noise generation, *Proceedings of the ASME Vibration Conference*, Las Vegas, 12-15, (1999).

[3] Feeny, B., Guran, A., Hinrichs, N., and Popp, K. A historical review on dry friction and stick-slip phenomena, *Appl. Mech. Rev.*, **51**, (1998).

[4] Hoffmann, N., Fischer, M., Allgaier, R., and Gaul, L. A minimal model for studying properties of the mode-coupling type instability in friction induced oscillations, *MRC*, **29**, 197-205, (2002).

[5] Hoffmann, N. and Gaul, L. Effects of damping on mode-coupling instability in friction induced oscillations, *ZAMM • Z. Angew. Math. Mech*., **83** (8), 524-534, (2003).

[6] Duffour, P. and Woodhouse, J. Instability of systems with a frictional point contact. Part 1: Basic modelling, *Journal of Sound and Vibration*, **271**, 365-390, (2004).

[7] Duffour, P. and Woodhouse, J. Instability of systems with a frictional point contacts. Part 2: Model extensions, *Journal of Sound and Vibration*, **271**, 391-410, (2004).

[8] D'Souza, A. F. and Dweib, A. H. Self-excited vibrations induced by dry friction, part 1: Experimental study, *Journal of Sound and Vibration*, **137** (2), 163-175, (1990).

[9] D'Souza, A. F. and Dweib, A. H. Self-excited vibrations induced by dry friction, part 2: Stability and limit-cycle analysis, *Journal of Sound and Vibration*, **137** (2), 177-190, (1990).

[10] Oden, J. T. and Martins, J. A. C. Models and computational methods for dynamic friction phenomena, *Computer Methods in Applied Mechanics and Engineering*, **52**, 527-634, (1985).

[11] Tworzydlo, W. W., Becker, E. B., and Oden, J. T. Numerical modelling of friction induced vibrations and dynamic instabilities, *ASME Applied Mechanics Review*, **47** (7), 255-274, (1994).

[12] Tworzydlo, W. W., Hamzeh, O. N., and Oden, J. T. Modelling and prediction of earthquakes as unstable phenomena of dynamic friction, technical report, *Computational Mechanics*, (in press).

[13] Leine, R. I., Brogliato, and Nijmeijer, B. H. Periodic motion and bifurcations induced by the Painleve paradox, *European Journal of Mechanics A/Solids*, **21**, 869-896, (2002).

[14] Pfeiffer, F. and Glocker, C. *Multibody Dynamics with Unilateral Contacts*, Wiley, New York, (1996).

[15] Song, P., Kraus, P., Kumar, V., and Dupont, P. Analysis of rigid-body dynamic models for simulation of systems with frictional contacts, *ASME Journal of Applied Mechanics*, **68**, 118-128, (2001).

[16] O'Malley Jr., R. E. *Singular Perturbation Methods for Ordinary Differential Equations*, Springer, New York, Berlin, (1991).

[17] Cottle, R. W., Pang, J. S., and Stone, R. E. *The Linear Complementarity Problem*, Academic Press, Inc., San Diego, CA, (1992).

[18] Hunt, K. H. and Crossley, F. R. E. Coefficient of restitution interpreted as damping in vibroimpact, *ASME Journal of Applied Mechanics*, June, 440-445, (1975).

[19] Marhefka, D. W. and Orin, D. E. A Compliant Contact Model with Nonlinear Damping for Simulation of Robotic Systems, *IEEE Trans. On Systems, Man, and Cybernetics - Part A: Systems and Humans*, **29** (6), 566-572, (1999).